Ultrafast and selective gas transport through highly ordered black phosphorene nanochannels

Yanqi Liu[a,b], Bo Jiang[c], Jiaming Luo[a,b], Jing Yang[a,b], Peichao Lian[a,b], Xinzhi Chen[a,b]*, Li Ding[d,]*, Yi Mei[a,b]*

[a] Yunnan Provincial Key Laboratory of Energy Saving in Phosphorus Chemical Engineering and New Phosphorus Materials, No.727 South Jingming Rd., Kunming, 650500, China

[b] Faculty of Chemical Engineering, Kunming University of Science and Technology, No.727 South Jingming Rd., Kunming, 650500, China

[c] Neutron Scattering Division, Oak Ridge National Laboratory Oak Ridge, Tennessee 37831, United States

[d] School of Chemistry and Chemical Engineering, South China University of Technology, Guangzhou, 510640, China

*** Corresponding author.** E-mail: xzchen001@hotmail.com, dingli@scut.edu.cn, meiyi412@126.com

Abstract:

Two-dimensional (2D) materials bring a great opportunity to fabricate molecular sieving membranes that can potentially break the permeability-selectivity trade-off. Although 2D laminar membranes with interlayer nanochannels as molecular sieving channel were widely studied, for most of reported 2D laminar membranes, it is of a great challenge to fabricate highly ordered interlayer nanochannels for mass transport. Herein, we report a novel kind of black phosphorene membrane which is made from the stacking of highly ordered 2D black phosphorene nanoflakes. The as prepared black phosphorene membrane shows H_2 permeance > 1000 GPU and H_2/CO_2 selectivity > 100 for H_2/CO_2 mixed gas, demonstrating an extremely high gas separation performance. The DFT calculation results demonstrate that the interlayer galleries in the black phosphorene membrane allow the H_2 passing through easily while block the other gases with bigger kinetic diameters, matching well with the experimental findings. The present results indicate that the interlayer galleries in the black phosphorene membrane can be applied as molecular sieving channels for gas separation.

Keywords: black phosphorus, black phosphorene, two-dimensional membrane, hydrogen separation, molecular sieving membrane

1. Introduction

Chemical separation process is an essential part in modern chemical industries. Conventional separation processes, such as distillation, consume 10-15 % of the world's energy [1]. Therefore, alternative separation technologies with low energy consumption is highly desired. Membrane-based separation technology has been regarded as a promising separation technology due to low energy consumption and simple crafts [2]. However, the separation performance of conventional membranes is generally suffered from the trade-off effect, high permeance and high selectivity are difficult to achieved simultaneously [2-4]. In consequence, it's of great interest to develop novel membranes that can break the trade-off effect to improve the separation performance.

The discovery of graphene has triggered great interest in investigating two-dimensional (2D) materials in various application fields [5-8]. Owing to their unique atomic thickness and extraordinary physicochemical properties, 2D materials have also received increasing attention as emerging building blocks for the next generation separation membranes [9-14]. To date, a number of work had been reported that membranes assembled by 2D materials including graphene-based materials, metal-organic frameworks (MOF), Zeolite, covalent organic frameworks (COF) and transition metal carbides (MXenes) delivered excellent gas separation performance [15-22]. Basically, the intrinsic or artificial pores in the monolayer nanoflake can be directly used as the main molecular sieving channels. For examples, Li et al reported that ultrathin GO membranes showed superior hydrogen separation selectivity (about 3400)

and the super high selectivity was suggested to be ascribed to the intrinsic defects in layered-GO laminates [23]. However, 2D materials with intrinsic pores are difficult to exfoliated successfully. In addition, it is cost-consuming and complex to make controllable and uniform artificial sub-nanopores in the monolayer 2D materials. Thus, the other kind of 2D laminar membranes attracted more attention, where the interlayer galleries between the adjacent nanoflakes play a role of the main molecular sieving channels. The stacking structure in the 2D laminar membranes significantly affects the separation performances. Take the graphene oxide (GO) membrane for example, randomly stacked GO membrane delivered poor separation performances because only the Knudsen diffusion worked during the separation process, while the orderly stacked GO membrane exhibited excellent gas separation performances because the orderly stacked GO nanoflakes constitutes molecular sieving channels [24, 25]. In addition, a laminar stacked MXene membrane with aligned and regular subnanometer channels was reported to have excellent gas separation with H_2 permeance > 2200 Barrer and H_2/CO_2 selectivity > 160 [26]. However, since the influence of functional groups adhered to the 2D nanoflakes, random stacking structure favors to form during the membrane assembly [25, 27]. Recently, a novel kind of 2D layered material named black phosphorene was first exfoliated from black phosphorus by Zhang's group in 2014 [28]. Some simulation work had shown that black phosphorene membranes possess excellent gas and ion separation potentials [29, 30]. Specifically, DFT results indicated that the monolayer porous black phosphorene membrane performed extremely high selectivity for hydrogen against other gas molecules such as N_2, CO,

CO_2, H_2O, and CH_4 in the order of 10^{13}, 10^{12}, 10^{15}, 10^{13}, and 10^{21}, respectively [31]. Therefore, it will be of great practical significance if the actual separation performances of the membrane can be verified experimentally. However, it should be noted that the DFT results are based on the model of the porous monolayer black phosphorene membrane (pore size 0.711 nm× 0.553 nm), which is very hard to be prepared by ordinary approaches. Nevertheless, we noted that the interlayer distance in black phosphorus is close to the pore size of the monolayer porous membrane, thus it is interesting to investigate the separation performances of the interlayer space channels in black phosphorus.

Herein, for the first time, we reported a novel kind of black phosphorene membrane whcih is made of highly ordered stacked black phosphorene nanoflakes. The black phosphorene membrane with aligned and regular subnanometer channels showed excellent hydrogen permeance (> 1000 GPU) and great selectivity (H_2/CO_2 > 100). The unique interlayer galleries in the black phosphorene membrane facilitate H_2 transport, leading to a high H_2 selectivity. DFT calculations revealed that the relative interaction energy of H_2 in layered black phosphorene interlayer gallery is as low as -3.5 eV, relative to other gas molecules system which have positive values. Therefore, the black phosphorene interlayer galleries allow H_2 passing through easily while block the other gases, leading to high gas permeance of H_2 against other gases. Such high hydrogen separation performances make the black phosphorene membranes favorable in many significant applications like hydrogen production and carbon dioxide capature.

2. Experimental

2.1 Preparation of bulk black phosphorus: The black phosphorus crystal was prepared by a mineralizer-assisted method using a short way transport reaction [32]. Specifically, the mixture of red phosphorus (500 mg, AR, purchased from Aladdin), Sn (80 mg, AR, purchased from Aladdin) and SnI_4 (30 mg, AR, purchased from Aladdin) was sealed in a silica tube and slowly heated up (5 ℃ min^{-1}) to the target temperature (600 ℃) in a muffle furnace, keeping at 600 ℃ for 6 hours and then gradually cooling down to 500 ℃, holding the temperature for 2 hours, then cooling down from 500 ℃ to room temperature, finally, the black phosphorus was obtained (Fig. S2).

2.2 Preparation of the black phosphorene nanosheets: 2D black phosphorene nanoflakes were obtained via ultrafast electrochemical cathodic expansion of home-made black phosphorus [33]. In detail, 1.2 g of tetrabutylammonium bromide (TBAB, AR, purchased from Aladdin) was dissolved in 20 mL acetonitrile (C_2H_3N, AR, purchased from Aladdin) as electrolyte. The black phosphorus was placed as the working cathode, and a Pt net was used as the counter electrode. A cathodic voltage lower than -5 V was applied, the black phosphorus was expanded in few minutes. After that, the expanded black phosphorus flakes were further exfoliated and dispersed in *N,N*-dimethylformamide (DMF, AR, purchased from Aladdin) solvent via ultrasonic cell disrupter at low power for 1.5 hour. The resulting suspension mixture was first centrifugated at 3000 rpm for 10 minutes to remove the un-exfoliated particles. Then the black phosphorene dispersion was washed using ultrapure water and centrifugated at 8000 rpm for 5 times to remove DMF solvent and remaining salts. A clean and

transparent suspension containing exfoliated black phosphorene nanoflakes was finally obtained.

2.3 Preparation of the black phosphorene membrane: 2D black phosphorene membranes were fabricated by filtering a certain amount of black phosphorene suspension on AAO (0.2 μm pore size and a diameter of 15 mm, purchased from Puyuannano Co., Ltd.) substrates using vacuum-assisted filtration. All membranes were dried at 20 ℃ for 24 hours.

2.4 Characterization of black phosphorene nanoflakes and the black phosphorene membranes: TEM images were obtained using a JEM-2100 plus microscope with an acceleration voltage of 200 kV. AFM images were obtained using a Bruker Dimension Icon scanning probe microscope in tapping mode. SEM images were obtained using Zeiss Sigma300 device. The SEM elemental mapping analysis was conducted using an EDX (Oxford EDS, with INCA software). The XRD analysis was carried out using a X'Pert 3 with filtered Cu-$K\alpha$ radiation (40 kV and 40 mA, λ=0.154 nm). The XPS analysis was performed using a Thermo Scientific K-Alpha+ spectrometer (Thermo Fisher Scientific) with monochromated Al-$K\alpha$ radiation (1486.6 eV) under a pressure of 5×10^{-9} mbar. Raman spectra was acquired at a spectral range of 300-800 cm^{-1} using an inVa Raman spectrometer equipped with a laser wavelength of 532 nm. The adsorption isotherms of H_2, CO_2, N_2, and CH_4 on black phosphorus powder were measured using a Micromeritics (ASAP 2460) instrument. The TG measurement was analyzed on a STA 449 instrument under the flow of N_2.

2.5 Gas permeation measurements: All the gas permeation measurements were

conducted in a home-made Wicke-Kallenbach permeation cell (Fig. S8). The gas flow rate was controlled by Mass Flow controllers (MFCs, Beijing HORIBA) and calibrated by a bubble flowmeter. A calibated gas chromatograph was used to analyze the composition of the permeate gas. The obtained membranes were sealed in a homemade membrane module to assess their separation performances. Silicone gaskets were placed on the both sides of the membranes to avoid the gas leakage. A calibrated gas chromatograph (GC, Fuli 9790II) equipped with a TCD and an FID detector was applied to analyze the gas compositions. Since the concentration of CO_2 in the permeation side is too low to be detected by a TCD detector, the permeation gas containing trace CO_2 pass through a methane reformer prior to entering the FID detector. During single-gas permeation, a flow rate of 50 mL min^{-1} gas was used in the feed side of the membrane, and sweep gas with a flow rate of 50 mL min^{-1} was used to carry the permeated gas into the GC instrument. During mixed-gas permeation, a gas mixture of H_2 and CO_2 with a ratio of 1:1 was applied at the feed side, and the total flow rate of the feed gas was maintained at 100 mL min^{-1}. The gas separation measurements were carried out at different temperatures. A heating tape was used to heat the membrane module with a heating rate of 2 °C min^{-1}. Feed gases containing various H_2 concentrations were obtained by adjusting the flow rates of H_2 and CO_2. All of the gas permeation tests were repeated at least three times to ensure accuracy. Gas permeance is calculated by the following Equation (1) [34]:

$$P_i = \frac{N_i}{A\Delta P_i} = \frac{F_i}{\Delta P_i} \quad (1)$$

where P_i is the permeance of component i (mol m^{-2} s^{-1} Pa^{-1}), N_i is the permeate rate of component i (mol s^{-1}), A is the effective membrane area (m^2), and ΔP_i is the transmembrane pressure difference of component i (Pa). Permeance can also be expressed as pressure normalized flux. F_i is the flux of component i (mol m^{-2} s^{-1}). In this paper, gas permeance is given in unit of GPU (Gas Permeation Unit), as the Equation (2).

$$1\ \text{GPU}=3.3928\times10^{-10}\ \text{mol}\ m^{-2}\ s^{-1}\ Pa^{-1} \quad (2)$$

The selectivity of two components in the single-gas permeation (ideal selectivity) was calculated by Equation (3)：

$$\alpha = \frac{P_i}{P_j} \quad (3)$$

The selectivity of two components in the mixed-gas permeation (separation factor) was calculated by Equation (4):

$$\alpha_{i/j} = \frac{y_i/y_j}{x_i/x_j} \quad (4)$$

where x and y are the volumetric fractions of the corresponding component in the feed and permeate side, respectively.

2.6 Computational methods: The first principle calculations were performed with the Vienna Ab initio Simulation Package (VASP) code [35, 36]. The standard projector augmented wave (PAW) method was used with VASP with electron wave functions

expanded in plane waves up to cutoff energy of 500 eV in this work. The Brillouin zone was sampled with k-point grid of 3×2×3 for a 2×1×2 supercell of black phosphorene. The convergence energy was set to 1×10^{-6} eV and the forces on the ions were relaxed until they were below 0.01 eV/Å. Full structural optimization was performed to black phosphorene firstly, and then the in-plane lattice constants were fixed for further calculations. Three kinds of exchange-correlation functional PBE, PBEsol and PBEsol using Van der Waals (vdW) corrections (DFT-D2) were tested for comparison as shown in Fig. S14 [37-39]. The applicability of PBE is general but PBEsol is more suitable to describe the properties of bulk solids and their surfaces. Previous computational study on the interlayer interaction suggests that the few layer black phosphorene is not a true van der Waals material [40]. To calculate the weak van der Waals (vdW) interactions between black phosphorene layers and molecular, the empirical correction of DFT-D2 that approximately accounts for dispersion interactions were applied. The binding energies for the black phosphorene layers are calculated as the energy difference of bulk and monolayer.

The relative energies (ΔE_{rel}) of various gas molecules embedded in layered black phosphorene as a function of the spacing of layers (spacing increased from 0.52 nm to 0.70 nm) were calculated by using Equation (5):

$$\Delta E_{rel} = E_{total} - E_{gas} - E_{phosphorene} \quad (5)$$

Where $E_{phosphorene}$ is the energy of the black phosphorene layers interlayer, and E_{gas} is the free state energy of gas molecules. E_{total} is the total energy of the gas molecules embedded black phosphorene layers structure.

3. Results and Discussion

3.1 Preparation and characterization of black phosphorene nanoflakes and black phosphorene membrane

Briefly, the black phosphorene nanoflakes were obtained by electrochemical intercalation and liquid exfoliation of black phosphorus [33]. After that, the black phosphorene nanoflakes solution was centrifuged and washed with ultrapure water, and then the obtained nanoflakes were re-dispersed in ultrapure water. Finally, the black phosphorene membrane was fabricated using vacuum-assisted filtration on a porous substrate (Fig. S1). As shown in Fig. 1a and Fig. S1a, a compact layer structure is obvious in the as prepared black phosphrus. The transmission electron microscopy (TEM) images show that the black phosphorene nanoflake is quite thin and nearly transparent to the electron beams (Fig. 1b and Fig. S3b). The corresponding lattice fringes of the black phosphorene nanoflakes can be clearly observed by high-resolution (HR) TEM (Fig. 1c), the (040) crystal plane of black phosphorus with lattice fringe spacing of 0.216 nm can be observed from the top view of the nanoflakes [41, 42]. Selected area electron diffraction (SAED) pattern in TEM model indicates high crystallinity of black phosphorene nanoflakes without obvious nanometer-scale defects (Fig. 1c, inset). Nanoparticle size analyzer was used to measure the nanosheet size distribution (Fig. S3d), most of black phosphorene nanoflakes lateral sizes are ranked in the range of 400 to 600 nm. Atom force microscope (AFM) was conducted to evaluate the thickness of black phosphorene nanoflakes. As shown in Fig. 1d, the observed black phosphorene nanoflakes exhibit a uniform thickness of 5.3 nm. Since

the theoretical thickness of a single layer phosphorene is about 0.2 nm [43-45], and considering that water molecules may be adsorbed by the phosphorene nanoflakes，which was verified by the FTIR result (Fig. S4), the 5.3 nm-thick phosphorene nanoflake should be few-layer phosphorene. From the top-view SEM image, the black phosphorene membrane is determined to be intact (Fig. 1e). A typical photograph of the black phosphorene membrane is shown in Fig. 1e inset and Fig. S6, the as-prepared black phosphorene membrane is flexible, and interestingly, the black phosphorene membrane has a metallic luster similar to that of the black phosphorus crystal, indicating that the black phosphorene membrane might possess a similar crystalline structure with black phosphorus crystal. The cross-sectional SEM image (Fig. 1f) reveals a well-organized, highly ordered laminar structure throughout the membrane and the thickness of the black phosphorene membrane is around 1.25 μm. To study the structure of the black phosphorene, the Raman spectra of black phosphorus and black phosphorus nanoflakes were compared. As shown in Fig. 1g, the black phosphorus exhibits three representative feature peaks centered at 357.5 cm^{-1}, 430.6 cm^{-1}, and 458.2 cm^{-1}, corresponding to the out-of-plane (A_g^1) and two in-plane (B_{2g} and A_g^2) phonon modes, respectively. While the Raman peaks of the black phosphorene nanoflakes are slightly blue-shifted for all the three modes. According to the first-principle calculation result done by Feng et al.[46], and previous experimental findings [47-49], due to the influence of covalent bonding, the P atoms collectively oscillate within the monolayer, as increasing the phosphorene layer, the oscillation of P atoms within the monolayer will be hindered owning to influence of the van der Waals forces from the adjacent P

atoms in the neighboring phosphorene layer, resulting in a red-shift in Raman spectrum. Thus, based on the experimental finding in our study, we speculate that the black phosphorus should be well exfoliated into few-layer phosphorene nanoflakes. The Tyndall scattering effect in the as- prepared black phosphorene colloidal suspension is clearly observed (Fig. S5). After exfoliation and self-assembly, the as prepared laminated membrane shows the similar XRD pattern with the pristine black phosphorus crystal (Fig. 1h), suggesting a maintained ordered crystal structure. The surface chemical compositions of black phosphorene membrane was analyzed by XPS, as shown in Fig. 1i. The characteristic P $2P$ doublet peaked at 129.8 and 130.6 eV corresponds to the P $2P_{3/2}$ and P $2P_{1/2}$ components, respectively. The black phosphorene membrane is thermally stable before 400 ^{o}C, which is simialr to the black phosphorus (Fig. S16).

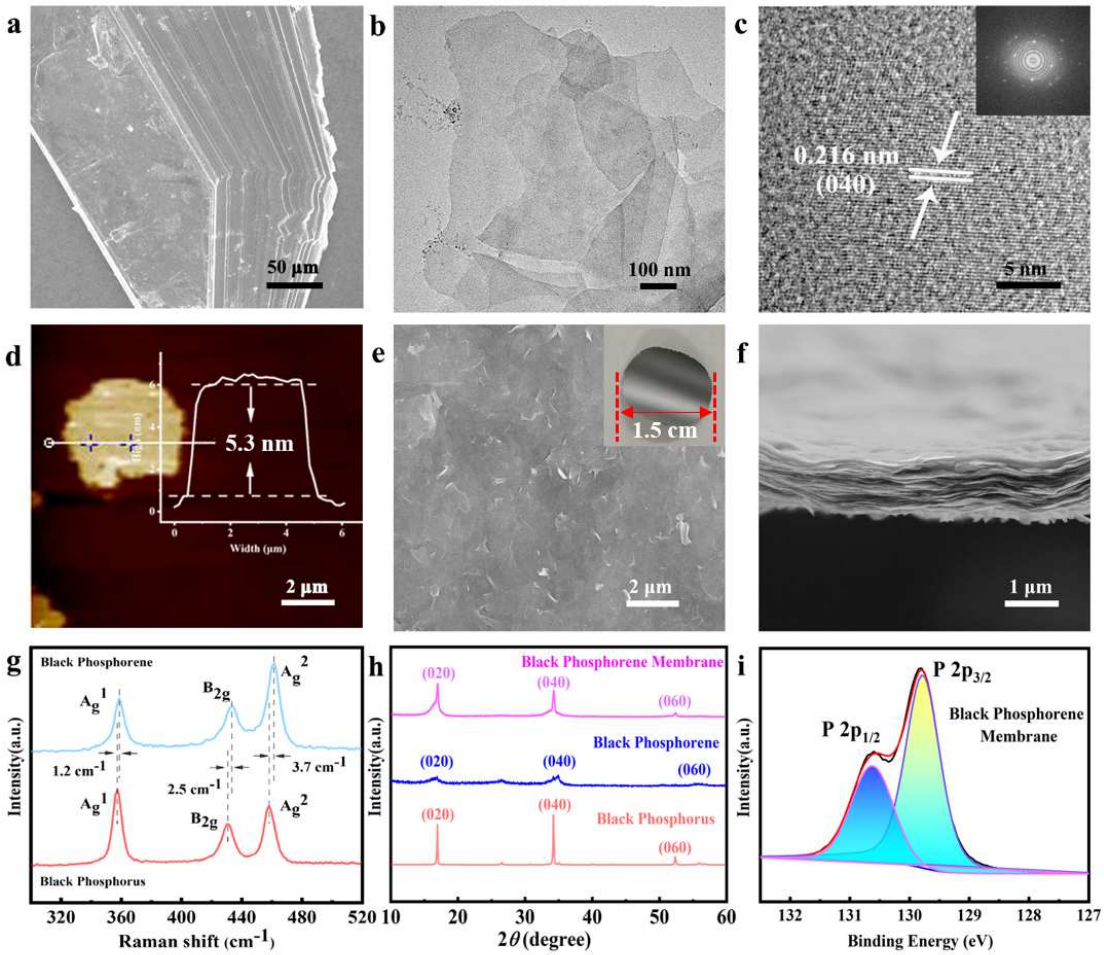

Fig. 1. (a) SEM image of black phosphorus. (b) TEM image of the black phosphorene nanoflakes. (c) HRTEM image of the black phosphorene nanoflake with SAED pattern in the inset. (d) AFM image of the black phosphorene nanoflake on cleaved mica. (e) SEM image of the black phosphorene membrane surface. Inset is a digital photograph of the black phosphorene membrane. (f) Cross-sectional SEM image of the BP membrane. (g) The Raman analysis of the black phosphorene and black phosphorus. (h) XRD patterns of the black phosphorus and the black phosphorene membrane. (i) High-resolution XPS spectra of P $2P$ for the black phosphorene membrane.

3.2 Gas separation performance of the black phosphorene membranes

Gas separation performance of the black phosphorene membranes were evaluated using an equimolar H_2/CO_2 mixture in a Wicke-Kallenbach permeation cell (Fig. S8). The quantitative analysis was performed by means of external standard method, and the standard calibration curves of gases were shown in Fig. S9. For a 1.25-μm-thick black phosphorene membrane, H_2 and CO_2 gas permeabilities are 808 GPU and 4.9 GPU (Fig. 2a), respectively, in the single gas permeation mode, resulting in an extremely high ideal selectivity of 164 (Fig. 2b). In the mixed gas permeation mode, H_2 and CO_2 gas permeabilities increase to 1015 GPU and 9 GPU (Fig. S10), respectively, suggesting a separation factor of 103 (Fig. 2b). Both the ideal selectivity and the separation factor of H_2/CO_2 are much higher than the Knudsen diffusion selectivity ($\sqrt{M_{co_2}/M_{H_2}} = 4.7$). On the one hand the gas permeance of small gas molecule H_2 is much higher than that of the gases with bigger kinetic diameters, indicating a clear cutoff between H_2 and the other gases. On the other hand the gas permeabilities decrease with the molecular weight, as shown in Fig. S11. Thus, both the gas kinetic diameter and the gas molecular weight dominate the gas permeation. Here it is noted that the gas molecules with bigger kinetic diameters, like CO_2, N_2, and CH_4, are not totally excluded from the laminar membrane due to the presence of the slit-like pores, resulting in detectable trace gas permeances and declined gas separation selectivity of H_2 against other gases. Since there is no intrinsic or artificial pore on the black phosphorene surface for gas transport, the slit-like pores provide rich mesoporous and microporous transporting channel. The slit-like pores allow gas molecules to enter the laminar membrane while the interlayer gallery can block gas molecules getting through except the gas with smaller kinetic

diameter like H_2. For the purpose of improving the gas separation selectivity, it is important to avoid the slit-like pores to form through-holes across the laminar membrane.

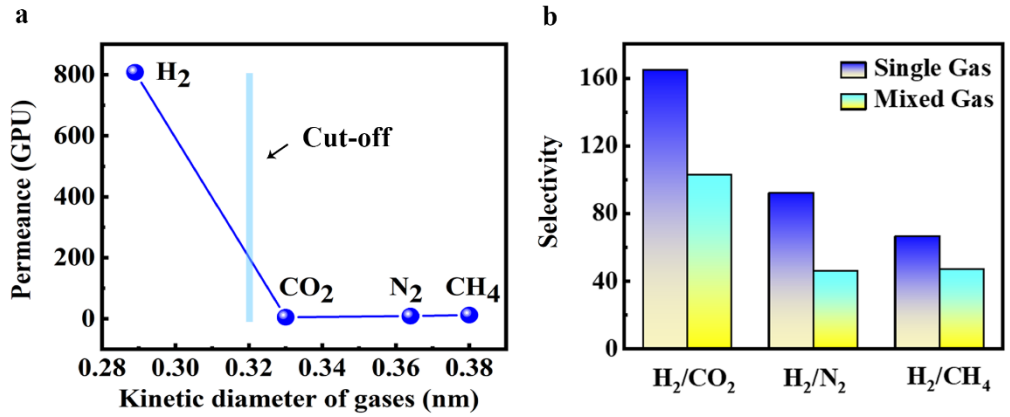

Fig. 2. Gas separation performances of a 1.25-μm-thick black phosphorene membrane at 20 °C and 0.1 MPa. (a) Gas permeabilities in the single gas permeation mode. (b) Comparison of the selectivity of H_2/CH_4, H_2/N_2, and H_2/CO_2 in the single gas and mixed-gas permeation modes.

3.3 Gas separation mechanism of the black phosphorene membrane

The X-ray diffraction (XRD) technique was applied to characterize the average distance of 2D channels in the laminar black phosphorene membrane. The interlayer gallery spacing can be approximately equal to the *d*-spacing calculated by using Bragg equation (Supplementary text 1.1). As shown in Fig. 1h, the characteristic peak of the pristine black phosphorus at 2θ=16.9° indicates that the initial *d*-spacing is about 0.52 nm, which is much larger than the kinetic diameters of N_2, CH_4, and CO_2 [50]. However, since the monolayer black phosphorene has two layers of phosphorus atoms, the practical interlayer gallery spacing should be lower than the calculated *d*-spacing.

According to the lattice parameters in the black phosphorus crystal, the theoritical thickness of a single layer phosphorene is about 0.2 nm [43-45], thus, the nearest parallel distance between the monolayer black phosphorene is about 0.32 nm. Considering that the kinetic diameters of H_2, CO_2, N_2 and CH_4 are 0.29 nm, 0.33 nm, 0.36 nm and 0.38 nm, respectively, the gas permeation thus can be ascribed to a molecular sieving (size exclusion) mechanism (Fig. 3a). While for the gases with the diameter larger than 0.32 nm, the permeation mechanism is considered as dissolution-diffusion [51, 52]. The adsorption isotherms of the gases on the black phosphorene membrane at 25 °C indicate a preferential adsorption of CH_4 compared to N_2 and CO_2 (Fig. 3b), which is consistent with the corresponding permeance (Fig. 2a). To further confirm the interactions between the tested gases and the black phosphorene nanochannel, DFT calculations were carried out to explore the corresponding energy barrieres. Previous DFT simulations revealed that the diffusion energy barriers of gas molecules passing through the porous monolayer black phosphorene membrane with a pore size of 0.711 nm ×0.553 nm varies with the kinetic diameter of various gas molecules. Specifically, the diffusion energy barrier for H_2 is almost negligible, leading to a superior gas separation selectivity in the order of 10^{13}, 10^{15} and 10^{21} for H_2 against N_2, CO_2, and CH_4 [31]. However, the black phosphorene membrane investigated in this work is different to the porous monolayer black phosphorene membrane, the previous DFT calculations are of limited guidance. Thus, a new DFT calculation model was performed with the Vienna Ab initio Simulation Package (VASP) code using the PBEsol functional [35-37, 39]. The relative interaction energies of various gas

molecules with layered black phosphorene were illustrated in Fig. 3c. It is noted that when the layer spacing is 0.52 nm (close to the original layer spacing of black phosphorus, the nearest distance between two monolayer black phosphorene is 0.32 nm), the relative interaction energy of H_2 molecule in layered black phosphorene is as low as to ~-3.5 eV, while the other gases show positive relative interaction energy values. This result suggests that the layered black phosphorene with the original layer spacing of black phosphorus shows much higher selectivity for H_2 agsinst other gases.

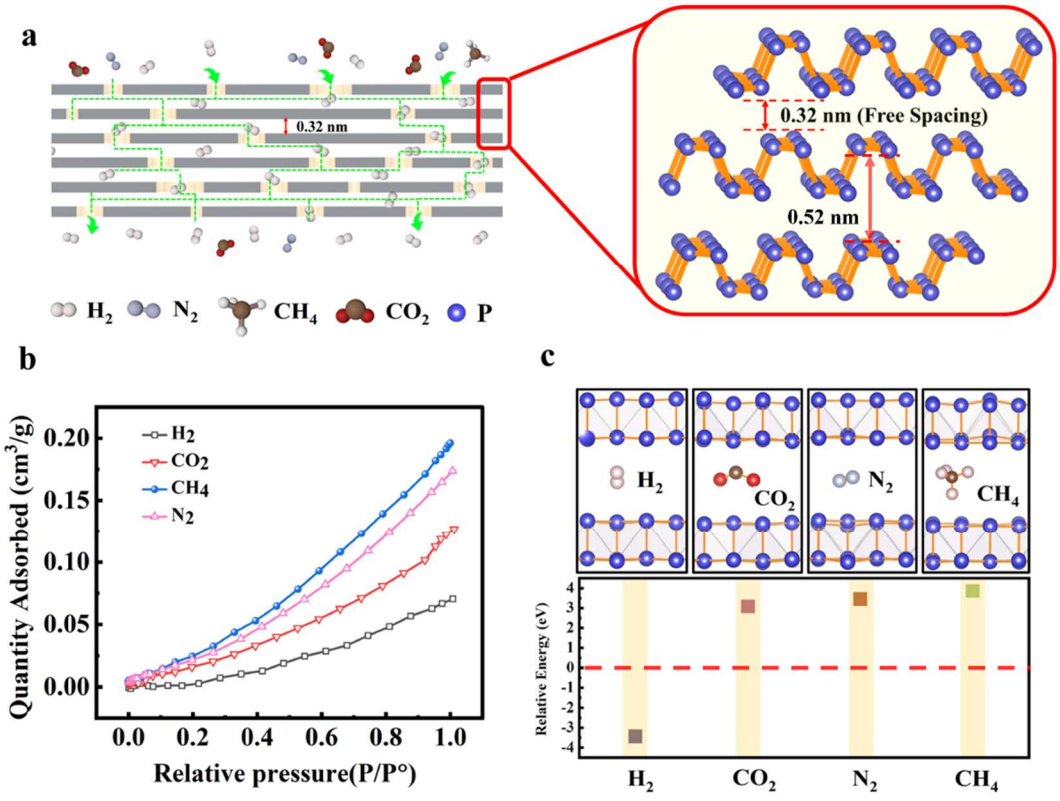

Fig. 3. (a) A presumed gas separation mechanism in the laminar black phosphorene membrane. (b) Adsorption isotherms of H_2, CO_2, N_2 and CH_4 on the black phosphorus at 20 °C. (c) The relative energy of various gas molecules in a DFT optimized black phosphorene layer structure.

3.4 Separation performances of the black phosphorene membrane under different test conditions

Moreover, the gas separation performance was further investigated by adjusting the temperature and feeding H_2 concentration (Fig. 4a, Fig. 4b, Fig. S12). It is worth noting that the permeate flux of H_2 slightly decreases with increasing temperature from 20 to 80 °C, while the permeate flux of CO_2 slightly increases, resulting in a declined selectivity. This finding suggests that the low temperature favors the improvement of H_2 separation performance. Even at a lower H_2 concentration in H_2/CO_2 mixture, both a high H_2 permeate flux and a high H_2 selectivity were achieved. The black phosphorene membrane shows stable gas separation performance during a 650 minnutes continuous separation of H_2/CO_2 mixture (Fig. 4c). Compared with various previously reported membranes (Fig. 4d, Supplementary Table S1), the black phosphorene membrane exhibits both excellent H_2 permeance (> 1000) and high H_2/CO_2 selectivity (> 100), which is ranked in the top level among state-of-the-art gas separation membranes. The promising separation performance is attributed to the unique layer structure in the black phosphorene membrane.

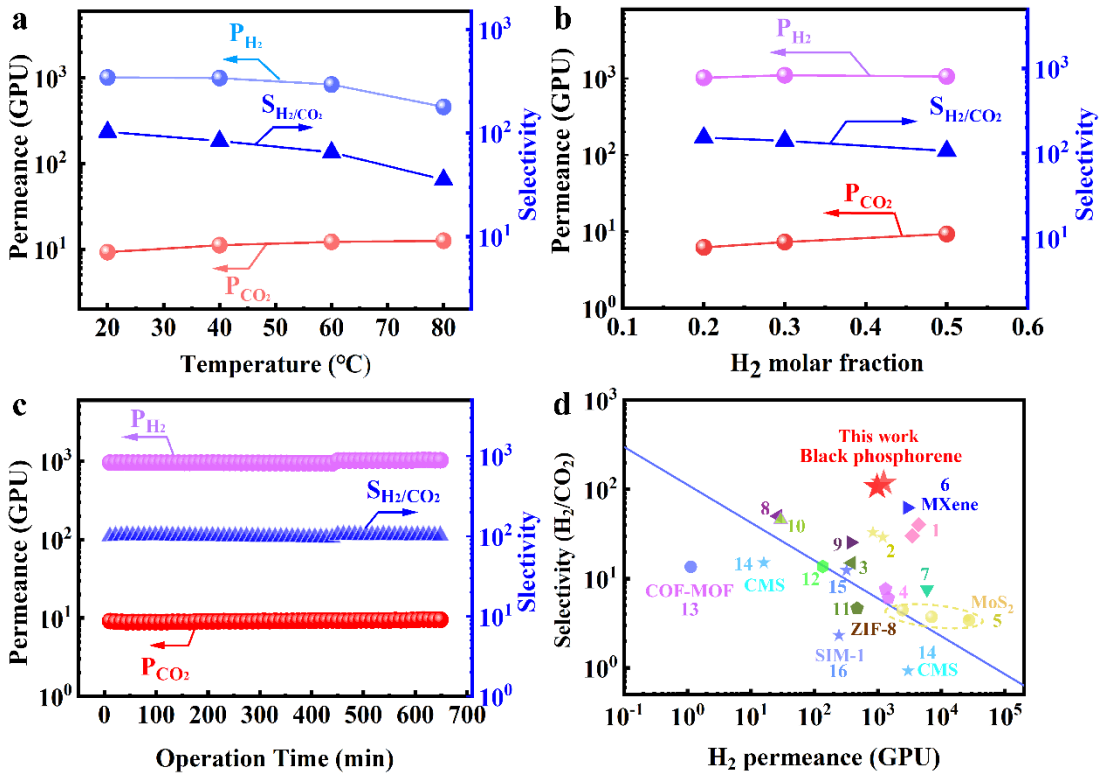

Fig. 4. (a) H_2/CO_2 separation performance of a 1.25-μm-thick black phosphorene membrane as a function of temperature in the equimolar mixed-gas permeation. (b) Effect of H_2 concentration in the feed mixed H_2/CO_2 gas on the separation performance of a 1.25-μm-thick black phosphorene membrane. (c) Long-term separation of equimolar H_2/CO_2 mixture through a 1.25-μm-thick black phosphorene membrane at 20 °C and 0.1 MPa. (d) H_2/CO_2 separation performance of the black phosphorene membrane compared with state-of-the-art gas separation membranes. The blue line indicates the Robeson 2008 upper bound of polymeric membranes for H_2/CO_2 separation. Information on the date points is given in Table S1.

4. Conclusions

In summary, a new function of 2D black phosphorus material was demonstrated, unlike the other 2D layered materials that normally form random laminar structure

when such 2D materials nanoflakes are stacked into membranes, the 2D black phosphorene membrane shows highly ordered crystal structure. The black phosphorene membrane exhibits both high H_2 permeance (> 1000 GPU) and great H_2/CO_2 separation selectivity (> 100), which is ranked in the top level among state-of-the-art gas separation membranes. The regular interlayer galleries in the black phosphorene membrane guarantee the outstanding H_2 separation selectivity, allowing H_2 to pass through while block the other gases. As such, the black phosphorene membrane is attractive for the H_2 purification process and CO_2 capture.

Declaration of Competing Interest

The authors declare no conflict of interest.

Acknowledgments

The research work reported in the paper was supported by the Natural Science Foundation of China (No. 21808065, 21968011). This research used resources of the Compute and Data Environment for Science (CADES) at the Oak Ridge National Laboratory, which is supported by the Office of Science of the U.S. Department of Energy under Contract No. DE-AC05-00OR22725.

References

[1] D.S. Sholl, R.P. Lively, Seven chemical separations to change the world, Nature 532(7600) (2016) 435-7.

[2] D.L. Gin, R.D. Noble, Designing the Next Generation of Chemical Separation Membranes, Science 332(6030) (2011) 674-676.

[3] B.D. Freeman, Basis of permeability/selectivity tradeoff relations in polymeric gas separation membranes, Macromolecules 32(2) (1999) 375-380.

[4] L.M. Robeson, Correlation of separation factor versus permeability for polymeric membranes, J. Membr. Sci. 62 (1991) 165-185.

[5] K.S. Novoselov, A.K. Geim, S.V. Morozov, D. Jiang, Y. Zhang, S.V. Dubonos, I.V. Grigorieva, A.A. Firsov, Electric field effect in atomically thin carbon films, Science 306(5696) (2004) 666-669.

[6] S.Z. Butler, S.M. Hollen, L. Cao, Y. Cui, J.A. Gupta, H.R. Gutierrez, T.F. Heinz, S.S. Hong, J. Huang, A.F. Ismach, E. Johnston-Halperin, M. Kuno, V.V. Plashnitsa, R.D. Robinson, R.S. Ruoff, S. Salahuddin, J. Shan, L. Shi, M.G. Spencer, M. Terrones, W. Windl, J.E. Goldberger, Progress, Challenges, and Opportunities in Two-Dimensional Materials Beyond Graphene, ACS Nano 7(4) (2013) 2898-2926.
[7] C.L. Tan, X.H. Cao, X.J. Wu, Q.Y. He, J. Yang, X. Zhang, J.Z. Chen, W. Zhao, S.K. Han, G.H. Nam, M. Sindoro, H. Zhang, Recent Advances in Ultrathin Two-Dimensional Nanomaterials, Chem. Rev. 117(9) (2017) 6225-6331.
[8] W. Huang, L. Hu, Y. Tang, Z. Xie, H. Zhang, Recent Advances in Functional 2D MXene-Based Nanostructures for Next-Generation Devices, Adv. Funct. Mater. 30(49) (2020).
[9] G.P. Liu, W.Q. Jin, N.P. Xu, Two-Dimensional-Material Membranes: A New Family of High-Performance Separation Membranes, Angew. Chem. Int. Edit. 55(43) (2016) 13384-13397.
[10] J.Y. Zhu, J.W. Hou, A. Uliana, Y.T. Zhang, M.M. Tian, B. van der Bruggen, The rapid emergence of two-dimensional nanomaterials for high-performance separation membranes, J. Mater. Chem. A 6(9) (2018) 3773-3792.
[11] Y.D. Cheng, Y.C. Pu, D. Zhao, Two-Dimensional Membranes: New Paradigms for High-Performance Separation Membranes, Chem. Asian J. 15(15) (2020) 2241-2270.
[12] F. Zhou, Q. Dong, J.-T. Chen, B. Sengupta, J. Jiang, W.L. Xu, H. Li, S. Li, M. Yu, Printed graphene oxide-based membranes for gas separation and carbon capture, Chem. Eng. J. 430 (2022).
[13] H. Yu, Y. He, G. Xiao, Y. Fan, J. Ma, Y. Gao, R. Hou, X. Yin, Y. Wang, X. Mei, The roles of oxygen-containing functional groups in modulating water purification performance of graphene oxide-based membrane, Chem. Eng. J. 389 (2020).
[14] Y. Zhou, Y. Zhang, J. Xue, R. Wang, Z. Yin, L. Ding, H. Wang, Graphene oxide-modified g-C3N4 nanosheet membranes for efficient hydrogen purification, Chem. Eng. J. 420 (2021).
[15] B. Elyassi, M. Sahimi, T.T. Tsotsis, Silicon carbide membranes for gas separation applications, J. Membr. Sci. 288(1-2) (2007) 290-297.
[16] D. Wang, Z.G. Wang, L. Wang, L. Hu, J. Jin, Ultrathin membranes of single-layered MoS2 nanosheets for high-permeance hydrogen separation, Nanoscale 7(42) (2015) 17649-17652.
[17] Y. Peng, Y.S. Li, Y.J. Ban, W.S. Yang, Two-Dimensional Metal-Organic Framework Nanosheets for Membrane-Based Gas Separation, Angew. Chem. Int. Edit. 56(33) (2017) 9757-9761.
[18] Y. Liu, Z.J. Chen, G.P. Liu, Y. Belmabkhout, K. Adil, M. Eddaoudi, W. Koros, Conformation-Controlled Molecular Sieving Effects for Membrane-Based Propylene/Propane Separation, Adv. Mater. 31(14) (2019) 7.
[19] H.W. Fan, M.H. Peng, I. Strauss, A. Mundstock, H. Meng, J. Caro, High-Flux Vertically Aligned 2D Covalent Organic Framework Membrane with Enhanced Hydrogen Separation, J. Am. Chem. Soc. 142(15) (2020) 6872-6877.
[20] Q.Q. Hou, S. Zhou, Y.Y. Wei, J. Caro, H.H. Wang, Balancing the Grain Boundary Structure and the Framework Flexibility through Bimetallic Metal-Organic Framework (MOF) Membranes for Gas Separation, J. Am. Chem. Soc. 142(21) (2020) 9582-9586.
[21] J. Shen, G. Liu, Y. Ji, Q. Liu, L. Cheng, K. Guan, M. Zhang, G. Liu, J. Xiong, J. Yang, W. Jin, 2D MXene Nanofilms with Tunable Gas Transport Channels, Adv. Funct. Mater. 28(31) (2018).
[22] E. Choi, S.J. Hong, Y.J. Kim, S.E. Choi, Y. Choi, J.H. Kim, J. Kang, O. Kwon, K. Eum, B. Han, D.W. Kim, Pore Tuning of Metal-Organic Framework Membrane Anchored on Graphene-Oxide Nanoribbon, Adv. Funct. Mater. 31(17) (2021).
[23] H. Li, Z.N. Song, X.J. Zhang, Y. Huang, S.G. Li, Y.T. Mao, H.J. Ploehn, Y. Bao, M. Yu, Ultrathin,

Molecular-Sieving Graphene Oxide Membranes for Selective Hydrogen Separation, Science 342(6154) (2013) 95-98.
[24] H.W. Kim, H.W. Yoon, S.M. Yoon, B.M. Yoo, B.K. Ahn, Y.H. Cho, H.J. Shin, H. Yang, U. Paik, S. Kwon, J.Y. Choi, H.B. Park, Selective Gas Transport Through Few-Layered Graphene and Graphene Oxide Membranes, Science 342(6154) (2013) 91-95.
[25] J. Shen, G.P. Liu, K. Huang, Z.Y. Chu, W.Q. Jin, N.P. Xu, Subnanometer Two-Dimensional Graphene Oxide Channels for Ultrafast Gas Sieving, ACS Nano 10(3) (2016) 3398-3409.
[26] L. Ding, Y.Y. Wei, L.B. Li, T. Zhang, H.H. Wang, J. Xue, L.X. Ding, S.Q. Wang, J. Caro, Y. Gogotsi, MXene molecular sieving membranes for highly efficient gas separation, Nat. Commun. 9 (2018) 7.
[27] W.W.L. Xu, C. Fang, F.L. Zhou, Z.N. Song, Q.L. Liu, R. Qiao, M. Yu, Self-Assembly: A Facile Way of Forming Ultrathin, High-Performance Graphene Oxide Membranes for Water Purification, Nano Lett. 17(5) (2017) 2928-2933.
[28] L.K. Li, Y.J. Yu, G.J. Ye, Q.Q. Ge, X.D. Ou, H. Wu, D.L. Feng, X.H. Chen, Y.B. Zhang, Black phosphorus field-effect transistors, Nat. Nanotechnol. 9(5) (2014) 372-377.
[29] J. Eke, K. Elder, I.C. Escobar, Self-Cleaning Nanocomposite Membranes with Phosphorene-Based Pore Fillers for Water Treatment, Membranes 8(3) (2018) 13.
[30] B. Du, X. Li, M. Xiao, The performance of nanoporous phosphorene as membranes for separating three typical C3F7CN insulating gas decomposition products, Appl. Surf. Sci. 537 (2021).
[31] Y.Y. Zhang, F. Hao, H. Xiao, C. Liu, X.Y. Shi, X. Chen, Hydrogen separation by porous phosphorene: A periodical DFT study, Int. J. Hydrog. Energy 41(48) (2016) 23067-23074.
[32] S. Li, X.Y. Liu, X. Fan, Y.Z. Ni, J. Miracle, N. Theodoropoulou, J. Sun, S. Chen, B. Lv, Q.K. Yu, New Strategy for Black Phosphorus Crystal Growth through Ternary Clathrate, Cryst. Growth Des. 17(12) (2017) 6579-6585.
[33] J. Li, C. Chen, S.L. Liu, J.P. Lu, W.P. Goh, H.Y. Fang, Z.Z. Qiu, B.B. Tian, Z.X. Chen, C.H. Yao, W. Liu, H. Yan, Y. Yu, D. Wang, Y.W. Wang, M. Lin, C.L. Su, J. Lu, Ultrafast Electrochemical Expansion of Black Phosphorus toward High-Yield Synthesis of Few-Layer Phosphorene, Chem. Mat. 30(8) (2018) 2742-2749.
[34] Y. Peng, Y.S. Li, Y.J. Ban, H. Jin, W.M. Jiao, X.L. Liu, W.S. Yang, Metal-organic framework nanosheets as building blocks for molecular sieving membranes, Science 346(6215) (2014) 1356-1359.
[35] Kresse, Furthmuller, Efficient iterative schemes for ab initio total-energy calculations using a plane-wave basis set, Physical review. B 54(16) (1996) 11169-11186.
[36] G. Kresse, D. Joubert, From ultrasoft pseudopotentials to the projector augmented-wave method, Phys. Rev. B 59(3) (1999) 1758-1775.
[37] J.P.B. Perdew, K.; Ernzerhof, M, Generalized Gradient Approximation Made Simple, Phys. Rev. Lett. 77(18) (1996) 3865-3868.
[38] S. Grimme, Semiempirical GGA-type density functional constructed with a long-range dispersion correction, J. Comput. Chem. 27(15) (2006) 1787-1799.
[39] J.P. Perdew, A. Ruzsinszky, G.I. Csonka, O.A. Vydrov, G.E. Scuseria, L.A. Constantin, X.L. Zhou, K. Burke, Restoring the density-gradient expansion for exchange in solids and surfaces, Phys. Rev. Lett. 100(13) (2008) 4.
[40] L. Shulenburger, A.D. Baczewski, Z. Zhu, J. Guan, D. Tománek, The Nature of the Interlayer Interaction in Bulk and Few-Layer Phosphorus, Nano Lett. 15(12) (2015) 8170-8175.
[41] A. Castellanos-Gomez, L. Vicarelli, E. Prada, J.O. Island, K.L. Narasimha-Acharya, S.I. Blanter, D.J. Groenendijk, M. Buscema, G.A. Steele, J.V. Alvarez, H.W. Zandbergen, J.J. Palacios, H.S.J. van der

Zant, Isolation and characterization of few-layer black phosphorus, 2D Mater. 1(2) (2014).
[42] D. Hanlon, C. Backes, E. Doherty, C.S. Cucinotta, N.C. Berner, C. Boland, K. Lee, A. Harvey, P. Lynch, Z. Gholamvand, S.F. Zhang, K.P. Wang, G. Moynihan, A. Pokle, Q.M. Ramasse, N. McEvoy, W.J. Blau, J. Wang, G. Abellan, F. Hauke, A. Hirsch, S. Sanvito, D.D. O'Regan, G.S. Duesberg, V. Nicolosi, J.N. Coleman, Liquid exfoliation of solvent-stabilized few-layer black phosphorus for applications beyond electronics, Nat. Commun. 6 (2015) 11.
[43] R. Hultgren, N.S. Gingrich, B.E. Warren, The Atomic Distribution in Red and Black Phosphorus and the Crystal Structure of Black Phosphorus, J. Chem. Phys. 3(6) (1935) 351-355.
[44] J.W. Jiang, H.S. Park, Negative poisson's ratio in single-layer black phosphorus, Nat. Commun. 5 (2014) 4727.
[45] D.K. Sang, H. Wang, Z. Guo, N. Xie, H. Zhang, Recent Developments in Stability and Passivation Techniques of Phosphorene toward Next-Generation Device Applications, Adv. Funct. Mater. 29 (2019) 1903419.
[46] Y. Feng, J. Zhou, Y. Du, F. Miao, C.G. Duan, B. Wang, X. Wan, Raman spectra of few-layer phosphorene studied from first-principles calculations, J. Phys. Condens. Matter 27(18) (2015) 185302.
[47] Z. Guo, H. Zhang, S. Lu, Z. Wang, S. Tang, J. Shao, Z. Sun, H. Xie, H. Wang, X.-F. Yu, P.K. Chu, From Black Phosphorus to Phosphorene: Basic Solvent Exfoliation, Evolution of Raman Scattering, and Applications to Ultrafast Photonics, Adv. Funct. Mater. 25(45) (2015) 6996-7002.
[48] A. Ambrosi, Z. Sofer, M. Pumera, Electrochemical Exfoliation of Layered Black Phosphorus into Phosphorene, Angew. Chem. Int. Edit. 56(35) (2017) 10443-10445.
[49] H. Xiao, M. Zhao, J. Zhang, X. Ma, J. Zhang, T. Hu, T. Tang, J. Jia, H. Wu, Electrochemical cathode exfoliation of bulky black phosphorus into few-layer phosphorene nanosheets, Electrochem. Commun. 89 (2018) 10-13.
[50] L. Ding, Y.Y. Wei, Y.J. Wang, H.B. Chen, J. Caro, H.H. Wang, A Two-Dimensional Lamellar Membrane: MXene Nanosheet Stacks, Angew. Chem. Int. Edit. 56(7) (2017) 1825-1829.
[51] H. Zhang, R. Guo, J. Zhang, X. Li, Facilitating CO2 Transport Across Mixed Matrix Membranes Containing Multifunctional Nanocapsules, ACS Appl. Mater. Interfaces 10(49) (2018) 43031-43039.
[52] Q. Gan, Y. Zou, D. Rooney, P. Nancarrow, J. Thompson, L. Liang, M. Lewis, Theoretical and experimental correlations of gas dissolution, diffusion, and thermodynamic properties in determination of gas permeability and selectivity in supported ionic liquid membranes, Adv. Colloid Interfac. 164(1-2) (2011) 45-55.

References

[1] J.P.B. Perdew, K.; Ernzerhof, M, Generalized gradient approximation made simple, Phys. Rev. Lett.77 (1996) 3865-3868.

[2] S. Grimme, Semiempirical GGA-type density functional constructed with a long-range dispersion correction, J. Comput. Chem. 27 (2006) 1787-1799.

[3] J.P. Perdew, A. Ruzsinszky, G.I. Csonka, O.A. Vydrov, G.E. Scuseria, L.A. Constantin, X.L. Zhou, K. Burke, Restoring the density-gradient expansion for exchange in solids and surfaces, Phys. Rev. Lett. 100 (2008) 13.

[4] H.W. Kim, H.W. Yoon, S.M. Yoon, B.M. Yoo, B.K. Ahn, Y.H. Cho, H.J. Shin, H. Yang, U. Paik, S. Kwon, J.Y. Choi, H.B. Park, Selective gas transport through few-layered graphene and graphene oxide membranes, Science 342 (2013) 91-95.

[5] J. Shen, G.P. Liu, K. Huang, Z.Y. Chu, W.Q. Jin, N.P. Xu, Subnanometer two-dimensional graphene oxide channels for ultrafast gas sieving, ACS Nano 10 (2016) 3398-3409.

[6] A.S. Huang, Q. Liu, N.Y. Wang, Y.Q. Zhu, J. Caro, Bicontinuous zeolitic imidazolate framework ZIF-8@GO membrane with enhanced hydrogen selectivity, J. Am. Chem. Soc. 136 (2014) 14686-14689.

[7] A. Achari, S. Sahana, M. Eswaramoorthy, High performance MoS2 membranes: effects of thermally driven phase transition on CO_2 separation efficiency, Energy Environ. Sci. 9 (2016) 1224-1228.

[8] D. Wang, Z.G. Wang, L. Wang, L. Hu, J. Jin, Ultrathin membranes of single-layered MoS_2 nanosheets for high-permeance hydrogen separation, Nanoscale 7 (2015) 17649-17652.

[9] L. Ding, Y.Y. Wei, L.B. Li, T. Zhang, H.H. Wang, J. Xue, L.X. Ding, S.Q. Wang, J. Caro, Y. Gogotsi, MXene molecular sieving membranes for highly efficient gas separation, Nat. Commun. 9 (2018) 1-7.

[10] R.M. de Vos, H. Verweij, High-selectivity, high-flux silica membranes for gas separation, Science 279 (1998) 1710-1711.

[11] B. Elyassi, M. Sahimi, T.T. Tsotsis, Silicon carbide membranes for gas separation applications, J. Membr. Sci. 288 (2007) 290-297.

[12] H.B. Wang, Y.S. Lin, Synthesis and modification of ZSM-5/silicalite bilayer membrane with improved hydrogen separation performance, J. Membr. Sci. 396 (2012) 128-137.

[13] Z. Tang, J.H. Dong, T.M. Nenoff, Internal surface modification of MFI-Type zeolite membranes for high selectivity and high flux for hydrogen, Langmuir 25 (2009) 4848-4852.

[14] X.F. Zhang, Y.G. Liu, S.H. Li, L.Y. Kong, H.O. Liu, Y.S. Li, W. Han, K.L. Yeung, W.D. Zhu, W.S. Yang, J.S. Qiu, New membrane architecture with high performance: ZIF-8 membrane supported on vertically aligned ZnO nanorods for gas permeation and separation, Chem. Mat. 26 (2014) 1975-1981.

[15] Y.S. Li, F.Y. Liang, H.G. Bux, W.S. Yang, J. Caro, Zeolitic imidazolate framework ZIF-7 based molecular sieve membrane for hydrogen separation, J. Membr. Sci. 354 (2010) 48-54.

[16] J.R. Fu, S. Das, G.L. Xing, T. Ben, V. Valtchev, S.L. Qiu, Fabrication of COF-MOF composite membranes and their highly selective separation of H_2/CO_2, J. Am. Chem. Soc. 138 (2016) 7673-7680.

[17] S.D. Kenarsari, D.L. Yang, G.D. Jiang, S.J. Zhang, J.J. Wang, A.G. Russell, Q. Wei, M.H. Fan, Review of recent advances in carbon dioxide separation and capture, RSC Adv. 3 (2013) 22739-22773.

[18] S.Y. Zhou, X.Q. Zou, F.X. Sun, H. Ren, J. Liu, F. Zhang, N. Zhao, G.S. Zhu, Development of hydrogen-selective CAU-1 MOF membranes for hydrogen purification by 'dual-metal-source' approach, Int. J. Hydrog. Energy 38 (2013) 5338-5347.

[19] S. Aguado, C.H. Nicolas, V. Moizan-Basle, C. Nieto, H. Amrouche, N. Bats, N. Audebrand, D. Farrusseng, Facile synthesis of an ultramicroporous MOF tubular membrane with selectivity towards CO_2, New J. Chem. 35 (2011) 41-44.

A novel black phosphorene molecular sieving membrane made of highly ordered black phosphorene nanoflakes is applied for hydrogen purification. The unique puckered interlayer galleries in the membrane facilitate hydrogen passing through, resulting in high hydrogen permeability and high hydrogen selectivity. The work demonstrated a molecular sieving function of black phosphorene material.

Yanqi Liu, Bo Jiang, Jiaming Luo, Jing Yang, Peichao Lian, Xinzhi Chen*, Li Ding* and Yi Mei*

Ultrafast and selective gas transport through highly ordered black phosphorene nanochannels